Short-range magnetic ordering in the highly frustrated pyrochlore $Y_2Mn_2O_7$

J. N. Reimers and J. E. Greedan
Institute for Materials Research and The McMaster Nuclear Reactor, McMaster University, Hamilton, Ontario, Canada, L8S 4M1

R. K. Kremer and E. Gmelin
Max-Planck-Institut für Festkörperforschung, Heisenbergstrasse 1, Postfach 90 06 65, 7000 Stuttgart 80, Federal Republic of Germany

M. A. Subramanian
E. I. du Pont de Nemours and Co., Experimental Station, Wilmington, Delaware 19898
(Received 20 August 1990)

The bulk magnetic susceptibility of $Y_2Mn_2O_7$ is suggestive of ferromagnetic order, with $\Theta_C = +41(2)$ K, and an apparent $T_c = 20$ K. However, both dc and ac susceptibility data show a broad maximum near 7 K, which is frequency and field dependent. Heat-capacity studies down to 2 K show no evidence for long-range magnetic order. Neutron-scattering data indicate the presence of both antiferromagnetic (first neighbors) and ferromagnetic (second and third neighbors) short-range correlations. These results are compared to mean-field-theory predictions for the highly frustrated 16*c* sites in the pyrochlore lattice. This material shows many properties in common with spin glasses in spite of the fact that there is no evidence for chemical disorder.

I. INTRODUCTION

Pyrochlore oxides have the chemical composition $A_2B_2O_7$ and crystallize in the cubic, face-centered space group $Fd\bar{3}m$, where the A and B atoms are metals located on the sites 16*d* and 16*c*, respectively, and the oxygens occupy the 48*f* and 8*a* sites. Each of the metal atoms in this system forms an infinite three-dimensional lattice of corner-sharing tetrahedra. If either the A or B atom is magnetic, then there is a very high degree of frustration when the nearest-neighbor interactions are antiferromagnetic. A schematic diagram of the tetrahedra formed by the 16*c* lattice within a unit cell is shown in Fig. 1. The 16*d* sublattice is identical to this except for a spatial displacement of $(\frac{1}{2},\frac{1}{2},\frac{1}{2})$.

In $Y_2Mn_2O_7$, Y^{3+} is diamagnetic and Mn^{4+} is a d^3 ion with a symmetric $^4A_2$ ground state in an octahedral environment. Thus, any anisotropy in this system is expected to be weak. However, because of the high level of frustration, weak effects may still be important for any ordering that takes place.

Crystallographic information on the series of compounds $R_2Mn_2O_7$ (R = Dy–Lu, Y) has been reported previously.[1] The cell parameter $a_0 = 9.901$ Å was determined by Guinier analysis for R = Y, and single-crystal x-ray diffraction showed no evidence for disorder. All of the $R_2Mn_2O_7$ compounds appear to be ferromagnetic from high-field susceptibility data, however, the authors still discuss the possibility of antiferromagnetic nearest-neighbor (NN) interactions for the Mn sublattice. The related compound $Y_2Mo_2O_7$ shows spin-glass-like behavior[2] in the form of a cusp and sample history dependence in the magnetic susceptibility, even though the compound is chemically ordered.[3] The high degree of frustration on the Mo^{4+} sublattice is believed to be responsible for these effects. Similar behavior has also been observed in susceptibility data for $Tb_2Mo_2O_7$.[4] Here spin-glass-like behavior is also evident in neutron-diffraction data where strong diffuse magnetic scattering develops below the apparent freezing temperature of 25 K. A more complete review of the magnetic properties of oxide pyrochlores can be found in Ref. 5. For a detailed discussion of magnetic ordering in pyrochlores as predicted by mean-field theory see Ref. 6.

Other systems relevant to this problem are the defect pyrochlores $CsMnFeF_6$ and $CsNiFeF_6$. In these compounds Cs is on the 8*b* sites and the two transition elements are disordered on the 16*c* sites.[7] Thus, there is a

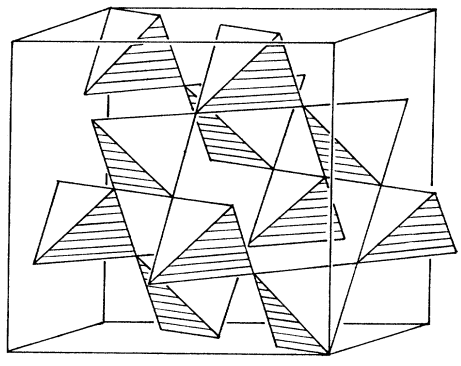

FIG. 1. The three-dimensional network of corner-sharing tetrahedra formed by the Mn^{4+} sublattice in $Y_2Mn_2O_7$. An outline of the cubic unit cell is also shown.

significant structural difference with the pyrochlore oxides which show no evidence for disorder on any site. Extensive measurements have been reported which indicate some behavior similar to that of spin glasses but also other effects which are contrary to such a characterization. Cusps in the low-field dc and ac susceptibility are reported along with differences in zero-field-cooled (ZFC) and field-cooled (FC) behavior, and remnant magnetism at low temperatures.[8,9] The specific heat for $CsNiFeF_6$ shows no maximum but a power law at low T, $C_m \propto T^{1.6}$, while $CsMnFeF_6$ has a maximum and a power-law behavior,[10] $C_m \propto T^{1.35}$. Neutron scattering discloses only diffuse features for $CsNiFeF_6$.[11] Diffuse scattering is also found for $CsMnFeF_6$ with one observation of very weak superimposed Bragg peaks[9] and another which observes only the diffuse scattering.[12]

In order to understand the nature of the low-temperature magnetic ordering and also to obtain some measure of the microscopic correlations present in $Y_2Mn_2O_7$, we have performed neutron-diffraction, magnetic susceptibility and heat-capacity measurements on a polycrystalline sample of $Y_2Mn_2O_7$. Comparisons will be made with the disordered flouride pyrochlores which might clarify the relative importance of frustration versus disorder in determining the magnetic properties of polychlore structure systems.

II. EXPERIMENTAL DETAILS

The preparation of polycrystalline $Y_2Mn_2O_7$ is described elsewhere.[1] $Y_2Sn_2O_7$ was prepared from a stoichimetric mixture of Y_3O_3 (99.99%, Research Chemicals, Lot No. Y-0-4-210) and SnO_2 (Specpure, Johnson Matthey, Lab No. 95080 ID) at 1400 °C in an aluminum oxide crucible.[13] After repeated grinding and firing for 1 day in air, the samples were found to be single phase by x-ray diffraction.

dc-susceptibility and magnetization data were measured with an SHE VTS (variable temperature SQUID) susceptometer. The powder samples were held in a quartz capsule and embedded in a fast-drying varnish to prevent reorientation of the grains. Zero-field-cooled runs were taken after cooling the sample in residual fields typically less than 0.02 mT. No corrections for demagnetization were applied.

ac-susceptibility data (χ' and χ'') were determined with a commercial CTI magnetometer in the frequency range 20–1000 Hz on powder samples which were pressed into a Delrin container.

Heat capacities were measured in an adiabatic calorimeter designed for the examination of small samples.[14] Powder samples with typical masses of 1g were sealed into Duran glass ampoules under He-exchange gas to provide sufficient thermal contact. The magnetic contribution C_m to the heat capacity of $Y_2Mn_2O_7$ was obtained after subtracting a lattice part which was calculated from the heat capacity of $Y_2Sn_2O_7$. For this purpose the heat capacity of $Y_2Sn_2O_7$ was converted into a temperature-dependent Debye temperature Θ_D according to the Debye law and carefully smoothed. The Debye temperature of $Y_2Sn_2O_7$ was then scaled by a factor of 1.08, chosen such that the heat capacities of $Y_2Mn_2O_7$ and $Y_2Sn_2O_7$ are equal above about 80 K.

The entropy was calculated from the magnetic heat capacity C_m by numerically integrating C_m/T following the thermodynamic relationship

$$S(T)=\int_0^T \frac{C_m}{T} dT \ . \tag{1}$$

The heat capacity below the lowest temperature reached by the experiment was estimated by extrapolating the linear T behavior found for C_m at higher T.

Powder neutron-diffraction data were obtained at the McMaster Nuclear Reactor with 1.3913-Å neutrons. Data sets at 200, 50, 25, 15, 10, and 7 K were collected. The detector was a three-tube position-sensitive detector which has been described previously.[3,15] The sample was held in an aluminum can along with helium-exchange gas and sealed with an indium gasket.

III. RESULTS AND DISCUSSION

A. dc-susceptibility and magnetization

The high-temperature susceptibility data were in good agreement with results published previously,[1] therefore, only essential facts are summarized here. For $T > 125$ K, χ_{mole} follows the Curie-Weiss (CW) law

$$\chi=\frac{C}{T-\Theta_c} \tag{2}$$

with $C=1.84(2)$ emu K/mol implying an effective magnetic moment of $\mu_{\text{eff}}=3.84(2)\mu_B$ or a spin value of $S=\frac{3}{2}$ as expected for Mn^{4+}. The paramagnetic Curie temperature amounts to $\Theta_c=41(2)$ K and indicates predominant ferromagnetic exchange interactions between Mn moments.

For $T < 125$ K deviations from the CW law appear. Below about 20 K a sudden rise in the magnetization is seen but the data are strongly dependent on the thermal history and the applied magnetic field (Fig. 2). A marked splitting of the ZFC and FC magnetization data is observed for small fields $B_{\text{ext}} < 10$ mT. While the FC mag-

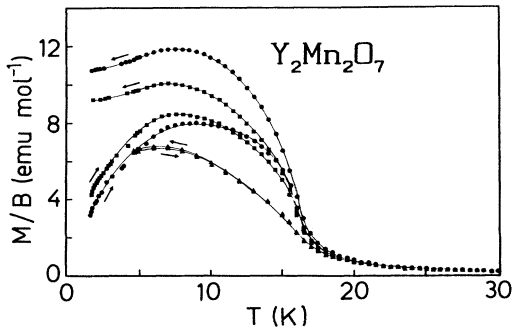

FIG. 2. Field-cooled (FC: ←) and zero-field-cooled (ZFC: →) dc-susceptibility of $Y_2Mn_2O_7$ per Mn atom. (●) 0.15 mT, (■) 0.56 mT and (▲) 10 mT.

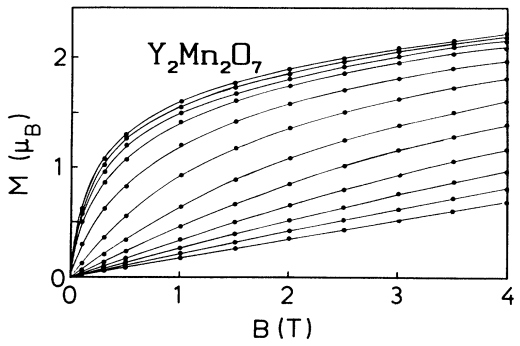

FIG. 3. High-field magnetization per Mn atom of $Y_2Mn_2O_7$ from top to bottom: at 1.8, 5, 7.5, 10, 15, 20, 25, 30, 35, 40, 45, and 50 K.

netization displays a weak maximum and saturates at a slightly lower value as $T \rightarrow 0$, the ZFC data go through a broad maximum and tend to zero. With increasing field the rise becomes flatter and the maxima decrease. The maximum shifts to lower temperatures and the splitting of FC and ZFC susceptibility is reduced upon increasing field. The difference between ZFC and FC susceptibility has almost completely vanished for $B_{ext} = 10$ mT. Above 10 K the data in Fig. 2 show behavior similar to that of a ferromagnet with spontaneous magnetization below a Curie temperature of about 20 K.

High-field measurements are shown in Fig. 3. Complete saturation cannot be achieved at 1.8 K in a field of 4 T. The magnetic moment per Mn atom is $2.3\mu_B$ and still considerably lower than $3\mu_B$ as expected for $S = \frac{3}{2}$. This gives strong support to the idea that antiferromagnetic correlations are present below 10 K.

Clearly there are some differences in detail between the disordered fluoride pyrocholores and the ordered oxide $Y_2Mn_2O_7$. $CsMnFeF_6$ and $CsNiFeF_6$ both display sharp dc-susceptibility cusps while the maximum for $Y_2Mn_2O_7$ is very broad in comparison. Yet both systems show similar ZFC and FC susceptibility curves. Of course, another major difference is that the fluorides are strongly antiferromagnetic with Θ_c values of -200 to -300 K while $Y_2Mn_2O_7$ has dominant ferromagnetic interactions $\Theta_c = 41$ K. In spite of this, the general features of the dc susceptibility are surprisingly similar.

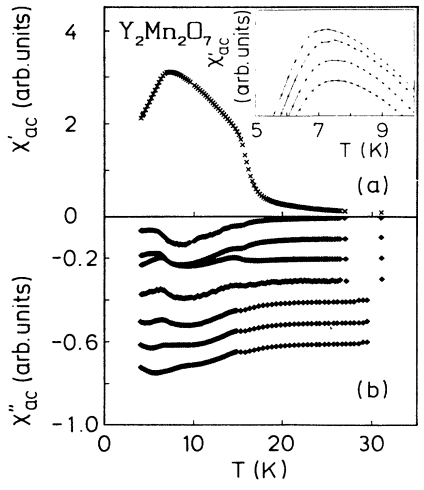

FIG. 4. ac-susceptibility of $Y_2Mn_2O_7$. (a) χ' at 20 Hz. The inset shows the χ' maxima for various frequencies, from top to bottom: 20, 100, 200, and 1000 Hz. (b) χ'' at various frequencies, from top to bottom: 20, 40, 80, 100, 200, 500, and 1000 Hz. Each curve was shifted by -0.1 compared to the preceding one.

B. ac-susceptibility

The shape of the temperature dependence of χ' measured at 20 Hz [Fig. 4(a)] is representative of the $\chi'(T)$ data for all other frequencies which were investigated. $\chi'(T)$ has some basic features in common with the dc-susceptibility, i.e., the relatively sharp rise below about 20 K and the maximum at about 7 K. Compared to the dc-susceptibility, however, the maximum is more pronounced and the data above the maximum fall into two ranges with different slopes. The slope change happens at about 15.5 K and simultaneously a kink in χ'' is generated.

The maxima temperatures are frequency dependent and shift to higher temperatures with increasing frequency (Fig. 5). The absorptive part of the ac-susceptibility, χ'', shows a stronger dependence on the frequency than χ' as displayed in Fig. 4(a). Besides the described kink at 15.5 K associated with the slope change in χ' a stronger mimimum occurs at slightly higher temperatures than the χ' maximum. With increasing frequency this minimum shifts, like the χ' maximum, to higher temperatures. At low temperatures an additional minimum gradually appears and superposes the high-temperature minimum. At 1000 Hz the low-temperature minimum is fully developed and represents the dominant feature in the temperature dependence of χ''.

The behavior of χ' and χ'' for $Y_2Mn_2O_7$ is significantly more complex than for the fluorides which show only a single χ' cusp feature with no anomalies above the cusp temperature. χ' (max) does shift to higher temperatures with increasing frequency for $CsNiFeF_6$ but $CsMnFeF_6$ does not show this effect. The feature at 15 K in

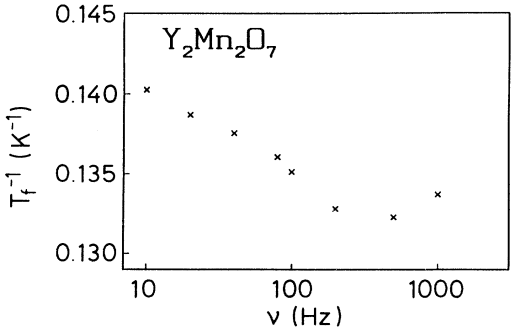

FIG. 5. Frequency dependence of the maximum temperature T_f of χ'.

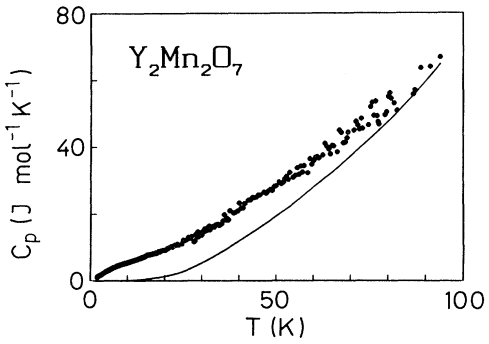

FIG. 6. Heat capacity of $Y_2Mn_2O_7$ (●). The solid line represents the scaled heat capacity of $Y_2Sn_2O_7$ which was used as a reference for the lattice heat capacity (see text for details).

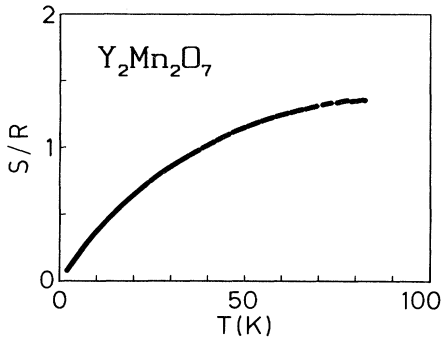

FIG. 8. Magnetic entropy of $Y_2Mn_2O_7$ per mole Mn. R is the molar gas constant.

$Y_2Mn_2O_7$ may be associated with ferromagnetic clusters which are absent in the largely antiferromagnetic fluorides. χ'' data have not been reported for $CsNiFeF_6$ or $CsMnFeF_6$. The data for $Y_2Mn_2O_7$ are remarkably complex and indicate a succession of changes in the magnetic microstructure as a function of temperature and frequency.

C. Heat capacity

The heat capacity of $Y_2Mn_2O_7$ shows no sharp anomaly usually associated with long-range magnetic ordering (Fig. 6). However, a comparison with the lattice heat capacity reveals a substantial magnetic contribution C_m due to short-range order. C_m is smeared out over a very large temperature range up to about 70 K. A broad maximum of C_m is centered around 40 K. Above 60 K the validity of the C_m data is diminished due to increasing scatter. At low temperatures, $T<7$ K, C_m follows a T^1 power law, $C_m=aT$, with $a=0.039(1)$ R (Fig. 7). In the interval 7 K $<T<20$ K, the data seem to follow another power law with an exponent less than unity, about 0.6–0.7. The change in power-law behavior at 7 K corresponds to the maximum in χ_{dc} and χ'_{ac}, below which antiferromagnetic correlations first set in.

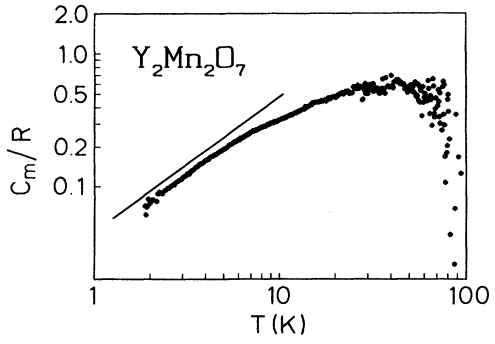

FIG. 7. Magnetic part C_m of the heat capacity for $Y_2Mn_2O_7$ per mole Mn. R is the molar gas constant. The solid line has slope unity.

The integrated entropy $S(T)$ presented in Fig. 8 reflects the peculiarities of C_m. $S(T)$ smoothly increases and almost saturates towards high temperatures. The saturation value 1.35 R is in good agreement with R ln4 expected for an $S=\frac{3}{2}$ magnetic system. At 18.4 K, where the magnetization data pointed to spontaneous magnetization, the entropy which has already been removed by short-range magnetic order amounts to about 55%.

A power-law temperature dependence is thus found for the pyrochlore systems with exponents ranging from 1.0 to 1.6 consistent with results found for traditional spin glasses.[16] The magnetic heat-capacity curves for $Y_2Mn_2O_7$ and $CsNiFeF_6$ are very similar, both showing a sharp break in slope at low temperature with no pronounced maximum, while $CsMnFeF_6$ shows a maximum.

D. Neutron-scattering data

No clear evidence for magnetic Bragg peaks was observed in the present study down to 7 K as seen in Fig. 9. Data were obtained elsewhere down to 2.5 K and very weak resolution-limited magnetic reflections were found at the (111) and (311) positions superimposed on a strong diffuse background and an additional weak reflection near $(\frac{1}{2},\frac{1}{2},\frac{1}{2})$.[17] Such a result was also found for $CsMnFeF_6$.[9] However, the complete absence of any specific-heat anomaly in $Y_2Mn_2O_7$ indicates that the long-range order component is exceedingly small and relatively unimportant compared to the dominant diffuse scattering. It is thus useful to concentrate on the analysis of the diffuse scattering and the short-range order which is implied.

Figure 9 shows the low-temperature data sets with the 200 K data subtracted in order to remove nuclear Bragg scattering and paramagnetic scattering. Small changes in the cell constants with temperature made it necessary to rescale Q-space for the 200 K data set at each temperature in such a way that the nuclear reflections would superimpose. This procedure is, of course, only valid for cubic systems. The rescaling is so slight as to have no effect on the diffuse magnetic scattering that is of interest. As the temperature is lowered, the magnetic scattering is

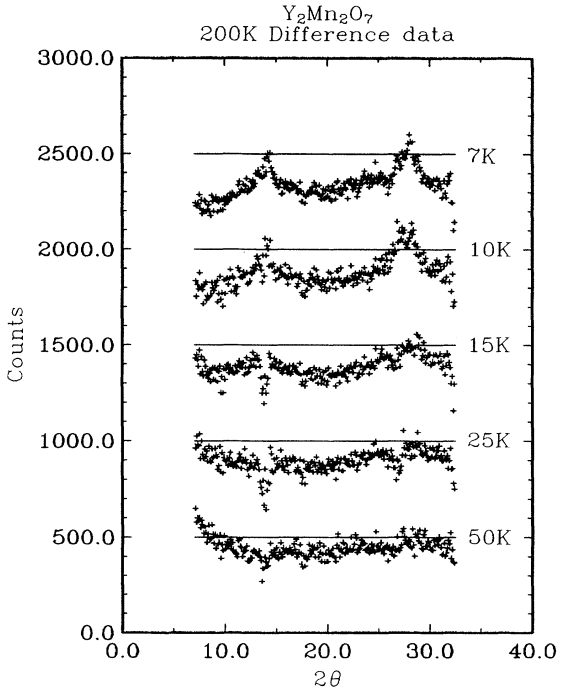

FIG. 9. Low-temperature neutron-diffraction data for $Y_2Mn_2O_7$ after subtracting the 200 K data.

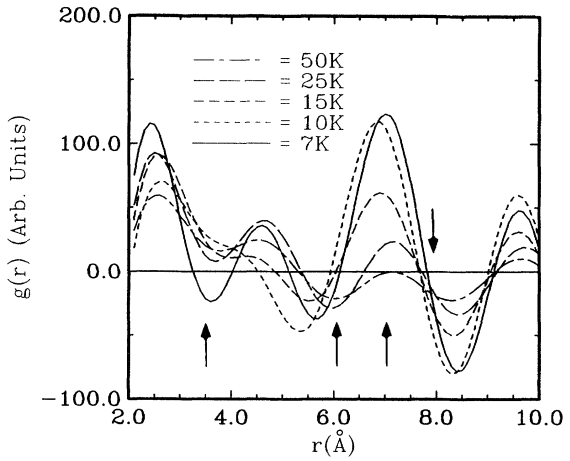

FIG. 10. Real-space radial correlation functions (in arbitrary units) obtained by Fourier transforming the low-temperature difference data sets. Arrows indicate the four nearest-neighbor bond distances for Mn sublattice.

seen to concentrate more and more near 14° and 27° in 2θ, which corresponds to d-spacings of 5.7 and 3.0 Å respectively. One can see by inspection that the Q-integrated scattering for all data sets is negative. This means that there must be a buildup of positive scattering somewhere outside the range of our data.

Better insight into the short-range correlations can be obtained by Fourier transforming the data, which gives the radial correlation function[18]

$$g(r)=\int_{Q_l}^{Q_h} I_{\text{diff}}(Q)f(Q)^{-2}Q\sin(Qr)dQ\ , \tag{3}$$

where $Q=4\pi\sin(\theta)/\lambda$ is the scattering vector, $I_{\text{diff}}(Q)$ is the magnetic scattering intensity at Q, with the paramagnetic scattering subtracted, and $f(Q)$ is the magnetic form factor. In the limit of isotropic interactions,

$$g(r)=\frac{1}{S(S+1)}\sum_{\mathbf{r}'}<\mathbf{S}_0\cdot\mathbf{S}_{\mathbf{r}'}>\delta(|\mathbf{r}|-|\mathbf{r}'|)\ , \tag{4}$$

which is a sum of spin-spin correlations at distance r. Figure 10 shows the Fourier transforms of the five low-temperature data sets. The arrows indicate the first four neighbor Mn-Mn bond distances. One can see that from 50 K down to 10 K ferromagnetic correlations are developing for the second and third coordination shells. This is consistent with the apparent ferromagnetic behavior observed in the high-temperature susceptibility. As a result of the highly frustrated nature of nearest-neighbor interactions on the Mn sublattice, only below 10 K is there any evidence for antiferromagnetic correlations for the first-neighbor coordination shell. The major limitation in this sort of analysis is most likely from the limited Q range of the data. Other sources of error such as data noise and anisotropy are less significant.

E. Comparison with Landau theory

Full details of the Landau theory for pyrochlores have been presented elsewhere.[6] Some results that are relevant to $Y_2Mn_2O_7$ will be discussed here. In order to simplify the calculations somewhat, the structure will be described in a nonstandard rhombohedral setting with a unit cell having one-quarter the volume of the cubic cell. The lattice vectors of the two systems are related by

$$\begin{bmatrix}\mathbf{a}\\ \mathbf{b}\\ \mathbf{c}\end{bmatrix}^{\text{rhom}}=\begin{bmatrix}0 & \frac{1}{2} & \frac{1}{2}\\ \frac{1}{2} & 0 & \frac{1}{2}\\ \frac{1}{2} & \frac{1}{2} & 0\end{bmatrix}\begin{bmatrix}\mathbf{a}\\ \mathbf{b}\\ \mathbf{c}\end{bmatrix}^{\text{cubic}}\ . \tag{5}$$

The advantage of the rhombohedral basis is that there are only 4 Mn^{4+} atoms per unit cell as opposed to 16 per cell in the cubic system. The corresponding space group is $R\bar{3}m$, which is a subgroup of $Fd\bar{3}m$. Thus, the rhombohedral representation has the disadvantage that some of the inherent symmetry is hidden. Table I shows a list of manganese-atom positions for both systems along with their nearest neighbors listed by atom number. The factor of 2 in front of each list of NN's indicates that there are two of each type of NN, which are related by spatial inversion. Following the notation in Ref. 6, we can write down the Landau free energy as follows:

$$F(T)=-\tfrac{1}{2}\sum_{i,j}\sum_{a,b}J_{ij}^{ab}\mathbf{B}_i^a\mathbf{B}_j^b+\frac{nT}{2}\sum_{i,a}(B_i^a)^2+O(B^4)\ , \tag{6}$$

where summations are over unit cells (i,j) and atoms within the unit cell (a,b), $\mathbf{B}_i^a=\langle\mathbf{S}_i^a\rangle$ are the thermal ex-

TABLE I. Manganese-atom positions in the rhombohedral and cubic basis, nearest neighbors are listed by atom number. FC stands for the face-centering operation (0,0,0; $0,\frac{1}{2},\frac{1}{2}$; $\frac{1}{2},0,\frac{1}{2}$; $\frac{1}{2},\frac{1}{2},0$).

Atom site	Atom no.	Position rhom	Position cubic	Nearest neighbors
16*c*	1	(0,0,0)	(0,0,0)+FC	2×(2,3,4)
16*c*	2	$(\frac{1}{2},0,0)$	$(0,\frac{1}{4},\frac{1}{4})$+FC	2×(1,3,4)
16*c*	3	$(0,\frac{1}{2},0)$	$(\frac{1}{4},0,\frac{1}{4})$+FC	2×(1,2,4)
16*c*	4	$(0,0,\frac{1}{2})$	$(\frac{1}{4},\frac{1}{4},0)$+FC	2×(1,2,3)

pectation values of the n-component unit spins, and the J's are exchange interactions. The first two terms in (6) are, respectively, the internal energy and the lowest-order entropy contribution. Entropy terms of order B^4 and higher will not be considered here as we are only concerned with nature of the highest-temperature ordered phase. After Fourier transforming (6), we have the free energy per unit cell.

$$f(T)=\tfrac{1}{2}\sum_{\mathbf{q}}\sum_{a,b}\mathbf{B}_q^a\cdot\mathbf{B}_{-\mathbf{q}}^b(nT\delta^{ab}-J_{\mathbf{q}}^{ab})+O(B^4)\ , \tag{7}$$

where

$$J_{\mathbf{q}}^{ab}=\sum_{i,j}J_{ij}^{ab}\exp[i\mathbf{q}\cdot(\mathbf{R}_i^a-\mathbf{R}_j^b)]\ , \tag{8}$$

$\mathbf{R}_i^a$ is an atom position, $\mathbf{q}$ is a wave vector in the first Brillouin zone, and δ^{ab} is a Kronecker δ. Because we are dealing with a non-Bravias lattice, Fourier transforming is not sufficient to diagonalize the second-order term, which dominates the free energy for small B_i. Transforming to normal modes (ϕ) of the system, we have

$$f(T)=\tfrac{1}{2}\sum_{\mathbf{q},i}|\phi_{\mathbf{q}}^i|^2(nT-\lambda_{\mathbf{q}}^i)+O(\phi^4)\ , \tag{9}$$

where $\lambda_{\mathbf{q}}^i$ are eigenvalues of $J_{\mathbf{q}}^{ab}$ and i now labels the normal modes. The first ordered state of the system will occur at a temperature

$$T_c=\frac{1}{n}\max\{\lambda_{\mathbf{q}}^i\}\ , \tag{10}$$

where max { } indicates a global maximum for all i and $\mathbf{q}$. Usually there will be a small number of symmetry-related $\mathbf{q}$ vectors characterizing the ordered state. The modes corresponding to max $\{\lambda_{\mathbf{q}}^i\}$ are sometimes referred to as critical modes or unstable modes (unstable because the corresponding $\mathbf{q}$-dependent susceptibility $\chi_{\mathbf{q}}$, diverges at T_c) of the system.

Using the information in Table I we have, for nearest-neighbor interactions,

$$J_{\mathbf{q}}^{ab}=2J_1\begin{bmatrix}0&\cos(q_x)&\cos(q_y)&\cos(q_z)\\ \cos(q_x)&0&\cos(q_x-q_y)&\cos(q_z-q_x)\\ \cos(q_y)&\cos(q_x-q_y)&0&\cos(q_y-q_z)\\ \cos(q_z)&\cos(q_z-q_x)&\cos(q_y-q_z)&0\end{bmatrix} \tag{11}$$

with eigenvalues

$$\begin{aligned}&\lambda_{\mathbf{q}}^1=\lambda_{\mathbf{q}}^2=-2J_1\ ,\\ &\lambda_{\mathbf{q}}^3=2J_1(1-\sqrt{1+Q}\,)\ ,\\ &\lambda_{\mathbf{q}}^4=2J_1(1+\sqrt{1+Q}\,)\ ,\end{aligned} \tag{12}$$

$$\begin{aligned}Q=\tfrac{1}{2}[&\cos(2q_x)+\cos(2q_y)+\cos(2q_z)\\ &+\cos(2q_x-2q_y)+\cos(2q_y-2q_z)\\ &+\cos(2q_z-2q_x)]\ .\end{aligned} \tag{13}$$

Note that λ^1 and λ^2 are completely independent of $\mathbf{q}$ and that these are the maximal eigenvalues for the system when $J_1<0$, which is the relevant case. Dispersion curves for the four modes are shown in Fig. 11, from which one can see that mode 3 is also degenerate with 1 and 2 at $\mathbf{q}=\mathbf{0}$. Thus, mean-field theory predicts a special temperature, $T_c=\frac{2}{3}|J_1|$ below which the system preferentially samples modes 1 and 2, i.e., half of phase space. This is consistent with our experimental result that 55% of the magnetic entropy in $Y_2Mn_2O_7$ is removed above 20 K (the temperature below which ferromagnetic correlations start to have effect). Because the system can sample a macroscopic number of Fourier modes below T_c, no long-range order is predicted within the mean-field approximation. One can understand this unusually high degree of degeneracy in terms of the strongly frustrated nature of antiferromagnetic ordering on a tetrahedron. The fact that the tetrahedra forming the Mn^{4+} sublattice are

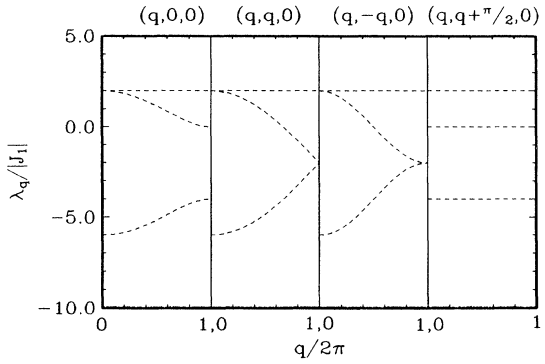

FIG. 11. Dispersion curves along certain symmetry directions for one sublattice pyrochlore systems with only NN exchange interactions. The unstable or critical modes will have the largest eigenvalue $\lambda_{\mathbf{q}}$ which is measured in units of J_1 the NN coupling constant.

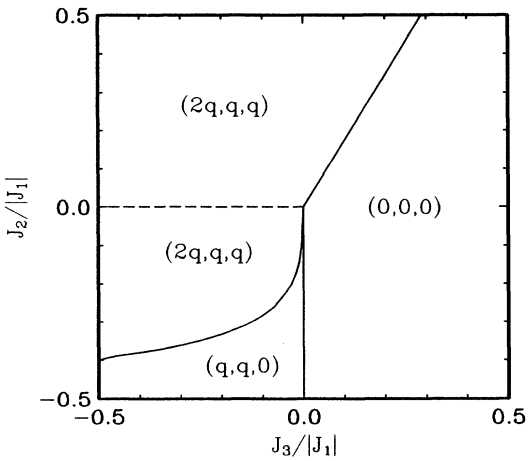

FIG. 12. Ordering wave vectors in the coupling parameter space J_3 and J_2 with $J_1=-1$. Along the dashed line, the system is continuously degenerate and critical along the $[q,q+(\pi/2),\pi/2]$ direction. For $Y_2Mn_2O_7$ we are concerned with the upper right-hand quadrant as directly indicated by the neutron-scattering data.

rather sparsely connected (corner sharing), as can be seen from Fig. 1, will also inhibit long-range order. Of course, weaker forces such as further neighbor interactions or dipole forces will lift some of this degeneracy but these forces will not be effective unless $T \ll J_1$.

The susceptibility data point towards strong ferromagnetic correlations which, from the neutron scattering, can be attributed to second- and third-neighbor interactions labeled as J_2 and J_3, respectively. Figure 12 shows the ordering wave vectors predicted by the Landau expansion in the parameter space of J_2 and J_3, with J_1 fixed at -1. For J_2 and $J_3>0$, the maxima in λ_q occurs at either $\mathbf{q}=\mathbf{0}$ or at an incommensurate point in the zone, depending on the J_2/J_3 ratio. On or near the phase boundary in this quadrant the maximum in λ_q is extremely weak and therefore thermal fluctuations will be strong, thus greatly depressing T_c. We have a situation where the exchange parameters are in competition and suppress long-range order, in spite of the fact the macroscopic degeneracy mentioned above has been lifted.

IV. SUMMARY AND CONCLUSIONS

In order to understand the magnetic properties of $Y_2Mn_2O_7$, one must realize that antiferromagnetic ordering in pyrochlores is extremely frustrated by the topology of the metal ion sublattice. In the absence of further neighbor interactions, such a system is not expected to order at any temperature.[19,20] Villain calls these systems "cooperative paramagnets."[20] The Landau-theory result explains this phenomenon in terms of a macroscopic degeneracy of the Fourier modes for all $\mathbf{q}$ vectors in the zone. As a result, the heat-capacity, high-field-magnetization, and neutron-diffraction data show no signs of significant long-range order in $Y_2Mn_2O_7$ down to 7 K.

The presence of further-neighbor ferromagnetic interactions can give misleading results for magnetic susceptibility data. In particular, the CW behavior at high temperatures and magnetization data from 10 to 20 K are both consistent with ferromagnetism. However, below 10 K, both the ac and dc susceptibility decrease as $T\rightarrow 0$, for ZFC samples, clearly indicating the presence of antiferromagnetic interactions. The inability of the magnetization to saturate at 1.8 K gives further support to this argument.

A number of results obtained on $Y_2Mn_2O_7$ are very similar to those found in disordered pyrochlores $CsNiFeF_6$ and $CsMnFeF_6$. These include (1) maxima in both the ac and dc susceptibility and sample-history-dependent behavior, (2) frequency dependence of χ', χ'', and χ'(max), (3) absence of features associated with long-range order in the heat capacity but the observation of a power law at low temperatures, and (4) removal of almost all the magnetic entropy by 2 K without long-range order. Many of these properties are associated with the spin-glass state. Similar behavior has been observed in other ordered oxide pyrochlores such as $Y_2Mn_2O_7$ (Ref. 2) and $Tb_2Mo_2O_7$.[4]

The temperature dependence of the magnetization, χ', and the neutron diffraction all resemble, to some degree, reentrant spin-glass behavior, of which $Eu_xSr_{1-x}S$ (Ref. 21) and $(Fe_xMn_{1-x})_{75}P_{16}B_6Al_3$ (Ref. 22) are good examples. These compounds, for a restricted range in x, show successive transitions from paramagnetism to ferromagnetism to spin-glass phases as the temperature is lowered. However, the ferromagnetism observed in $Y_2Mn_2O_7$ extends over relatively short distances contrary to $Er_xSr_{1-x}S$ where magnetic Bragg peaks in the neutron scattering are observed in ferromagnetic regime.

From evidence, it is clear that the high degree of frustration in $Y_2Mn_2O_7$ leads to unusual magnetic properties. It seems that the nature of the Mn sublattice is, at least in part, responsible for spin-glass-like behavior. A more sophisticated treatment of the problem than the Landau theory presented would be required to predict spin-glass behavior. Work along these lines may give some insight as to the role that frustration plays in the spin-glass problem.

ACKNOWLEDGMENTS

We thank Dr. M. Hartwig for carrying out the ac-susceptibility measurements and M. Gehrke for his help with the dc-susceptibility. J.N.R. and J.E.G. acknowledge financial assistance from the Natural Science and Engineering Research Council of Canada.

[1]M. A. Subramanian, C. C. Torardi, D. C. Johnson, J. Pannetier, and A. W. Sleight, J. Solid State Chem. **72**, 24 (1988).
[2]J. E. Greedan, M. Sato, X. Yan, and F. S. Razavi, Solid State Commun. **59**, 895 (1986).
[3]J. N. Reimers and J. E. Greedan, J. Solid State Chem. **72**, 390 (1988).
[4]J. N. Reimers, J. E. Greedan, S. L. Penny, and C. V. Stager, J. Appl. Phys. **67**, 5967 (1990).
[5]J. E. Greedan, in *Magnetic Pyrochlore Oxides,* edited by H. P. J. Wijn, Landholt-Bornstein, New Series, Group 27, Vol. III, (Springer-Verlag, Berlin, unpublished).
[6]J. N. Reimers, A. J. Berlinsky, and A.-C. Shi, Phys. Rev. B **43**, 3387 (1991).
[7]D. Babel, Z. Anorg. Allg. Chem. **387**, 161 (1972).
[8]M. Alba, J. Hammann, C. Jacoboni, and C. Pappa, Phys. Rev. Lett. **89A**, 423 (1982).
[9]L. Bevaart, P. M. H. L. Tegelaar, A. J. van Duyneveldt, and M. Steiner, Phys. Rev B **26**, 6150 (1982).
[10]C. Pappa, J. Hammann, and C. Jacoboni, J. Magn. Magn. Mater. **31-34**, 1391 (1983).
[11]C. Jacoboni, Ph.D. thesis, Université de Paris VI, 1975.
[12]W. Kurtz and S. Roth, Physica B **86-88**, 715 (1977); W. Kurtz, R. Geller, H. Dachs, and P. Convert, Solid State Commun. **18**, 1479 (1976).
[13]O. Knop, F. Brisse, L. Castelliz, and Sutarno, Can. J. Chem. **43**, 2812 (1965); F. Brisse and O. Knop, *ibid.* **46**, 859 (1986).
[14]E. Gmelin and K. Ripka, Cryogenics **21**, 177 (1981); W. Dai, E. Gmelin, and K. Ripka (private communication).
[15]J. N. Reimers, J. E. Greedan, and M. A. Subramanian, J. Solid State Chem. **79**, 263 (1989).
[16]K. Binder and A. P. Young, Rev. Mod. Phys. **58**, 801 (1986).
[17]J. Pannetier (unpublished).
[18]E. F. Bertaut and P. Burlet, Solid State Commun. **5**, 279 (1967).
[19]P. W. Anderson, Phys. Rev. **102**, 1008 (1956).
[20]J. Villain, Z. Phys. B **33**, 31 (1978).
[21]M. A. Manheimer, S. M. Bhagat, and H. S. Chen, J. Magn. Magn. Mater. **38**, 147 (1983).
[22]H. Maletta and W. Felsch, Z. Phys. B **37**, 55 (1980).